Integration of Merged Delayed-Enhanced Magnetic Resonance Imaging and Multi-Detector Computed Tomography for the Guidance of Ventricular Tachycardia Ablation – A Pilot Study

Hubert Cochet MD *‡, Yuki Komatsu MD †‡, Frederic Sacher MD †‡, Amir Sherwan Jadidi MD †‡, Daniel Scherr MD †‡, Matthieu Riffaud MD *, Nicolas Derval MD †‡, Ashok Shah MD †‡, Laurent Roten MD †‡, Patrizio Pascale MD †‡, Jatin Relan PhD §, Maxime Sermesant PhD §, Nicholas Ayache PhD §, Michel Montaudon MD, PhD *‡, François Laurent MD *‡, Mélèze Hocini MD †‡, Michel Haïssaguerre MD †‡, Pierre Jaïs MD, PhD †‡

Short Title: MDCT/MRI fusion for the guidance of VT ablation

Affiliations:

* Department of cardiovascular imaging, CHU / Université de Bordeaux, Pessac, France.

† Department of cardiac pacing and electrophysiology, CHU / Université de Bordeaux, Pessac, France.

‡ L'Institut de Rythmologie et de Modélisation Cardiaque LIRYC, CHU / Université de Bordeaux / INSERM U1045, Pessac, France.

§ INRIA Asclepios research team – INRIA Sophia Antipolis, Sophia Antipolis, France.

Funding: This research is supported by a grant from Fondation Leducq (09 CVD 03)

Relationship with industry: Pr. Jaïs is a speaker and consultant for St Jude Medical and Biosense Webster. Pr. Haissaguerre is a consultant for Biosense Webster. Dr. Sacher is a consultant for Biosense Webster.

Address for correspondence: Dr. Hubert Cochet, Departement d'imagerie cardiovasculaire, Hopital cardiologique Haut Lévêque, CHU Bordeaux. 33604 Pessac, France.

Tel: +33557656542, Fax: +33557656880, e-mail: hcochet@wanadoo.fr

Abstract

Background: Delayed enhancement (DE) MRI can assess the fibrotic substrate of scar-related VT. MDCT has the advantage of infra-millimetric spatial resolution and better 3D reconstructions. We sought to evaluate the feasibility and usefulness of integrating merged MDCT/MRI data in 3D-mapping systems for structure-function assessment and multimodal guidance of VT mapping and ablation.

Methods: Nine patients, including 3 ischemic cardiomyopathy (ICM), 3 non ischemic cardiomyopathy (NICM), 2 myocarditis and 1 redo procedure for idiopathic VT, underwent MRI and MDCT before VT ablation. Merged MRI/MDCT data were integrated in 3D-mapping systems and registered to high density endo- and epicardial maps. Low voltage areas (<1.5mV) and local abnormal ventricular activities (LAVA) during sinus rhythm were correlated to DE at MRI, and wall-thinning (WT) at MDCT.

Results: Endo- and epicardium were mapped with 391±388 and 1098±734 points/map, respectively. Registration of MDCT allowed visualization of coronary arteries during epicardial mapping/ablation. In the idiopathic patient, integration of MRI data identified previously ablated regions. In ICM patients, both DE at MRI and WT at MDCT matched areas of low voltage (overlap 94±6 and 79±5%, respectively). In NICM patients, wall-thinning areas matched areas of low voltage (overlap 63±21%). In patients with myocarditis, sub-epicardial DE matched areas of epicardial low voltage (overlap 92±12%). A total number of 266 LAVA sites were found in 7/9 patients. All LAVA sites were associated to structural substrate at imaging (90% inside, 100% within 18mm).

Conclusion: The integration of merged MDCT and DEMRI data is feasible and allows combining substrate assessment with high spatial resolution to better define structure-function relationship in scar-related VT.

Keywords: Ventricular tachycardia – Ablation – Image integration – Magnetic Resonance Imaging – Multi-Detector Computed Tomography – Multimodality

Abbreviations

CS = coronary sinus

DEMRI = delayed-enhancement magnetic resonance imaging

GZ = gray zone

ICD = implantable cardioverter defibrillator

ICM = ischemic cardiomyopathy

LAVA = local abnormal electrical activity

MDCT = multi-detector computed tomography

NICM = non-ischemic cardiomyopathy

VT = ventricular tachycardia

WT = wall thinning

INTRODUCTION

The majority of ventricular tachycardias (VT) is observed in structurally diseased hearts showing fibrotic scar (1). Surviving muscle fibers within fibrosis display slow conduction properties that may lead to reentrant circuits and subsequent tachycardia (2,3). In patients resistant to anti-arrhythmic drugs, catheter ablation can be performed to interrupt the reentrant circuit (4). Ideally, mapping of inducible, well-tolerated monomorphic VT allows for the identification of a critical isthmus amenable to catheter ablation. When the tachycardia is not inducible or non-mappable, VT substrate can be estimated using contact mapping as low voltage areas (5,6), or poorly coupled surviving fibers within scar generating local abnormal ventricular activities (LAVA) (7,8). Myocardial scar imaging with the use of MRI has been proposed as an additional method to guide ablation, and a substantial correlation has already been demonstrated between areas of DE at MRI and low voltage at contact mapping (9-12). The ability to locate myocardial scar could potentially reduce procedure time by focusing the mapping on previously defined areas. However, some patients with structural heart disease do not show DE at MRI because the method cannot depict diffuse interstitial remodeling (13). On the other hand, wall thinning (WT) at contrast-enhanced ECG-gated cardiac MDCT has been shown to correlate with low voltage (14), and the integration of MDCT coronary angiography might be valuable to guide epicardial ablation (15). This pilot study aims at (i) demonstrating that MDCT and MRI can be fused to combine substrate assessment with infra-millimetric spatial resolution, (ii) comparing VT substrate assessment with MDCT and MRI in ischemic and non-ischemic heart disease, (iii) correlating these structural data to electrical function using endocardial and epicardial high-density voltage and LAVA maps.

METHODS

Population

From March to October 2011, consecutive patients referred for catheter ablation of VT were prospectively enrolled. Exclusion criteria were contra-indications to gadolinium-enhanced MRI and iodine-enhanced MDCT. On a total of 31 VT ablation procedures, 23 patients were excluded because of the presence of an ICD contra-indicating MRI. Eight patients were included (6 men, age 47.5±13.6 years). In 6 patients (3 ICM, 3 NICM), the indication for ablation was sustained monomorphic VT resistant to optimal anti-arrhythmic medication and scheduled for ICD implantation. In one patient (male, age 31) with history of sustained monomorphic VT and recent viral myocarditis, catheter ablation was proposed as an alternative to amiodarone therapy and ICD implantation. One patient (female, age 36) with idiopathic septal VT was referred for redo because of arrhythmia recurrence following previous ablation. The study was approved by our Institutional Ethics Committee. All patients gave written informed consent.

Image acquisition

MRI was performed 1-3 days before ablation on a 1.5 T clinical scanner equipped with a 32-channel cardiac coil (Avanto, Siemens Medical Solutions, Erlangen, Germany). DE imaging was performed using a free-breathing method initially developed for atrial scar imaging (16), in order to study myocardial scar at high spatial resolution (voxel size 1.25x1.25x2.5mm, reconstructed to 0.625x0.625x2.5mm after inplane interpolation). This 3-dimensional, inversion-recovery-prepared, ECG-gated, respiration-navigated gradient-echo pulse sequence with fat-saturation was initiated 15 min after intravenous injection of 0.04 mmol/Kg gadopentate dimeglumine (Guerbet, Aulnay-sous-bois, France), and preceded by a TI-scout scan to define the optimal inversion time to null the signal in healthy myocardium. Contrast-enhanced ECG-gated cardiac MDCT was performed immediately after MRI study on a 64-slice CT scanner (SOMATOM Definition, Siemens Medical Solutions, Forchheim, Germany). Patients were placed supine, arms along the body, in the same position as the one

used for MRI. Images were acquired during an expiratory breath hold with tube current modulation set on end-diastole. CT angiographic images were acquired during the injection of a 120 mL bolus of iomeprol 400 mg I/ml (Bracco, Milan, Italy) at a rate of 4mL/s, and reconstructed at the same phase as the one used for DE imaging.

Image processing

The image processing method is illustrated in Figure 1. Point-based registration between MDCT and MRI series was achieved by one observer (HC, 7 years experience in cardiac imaging) using the software OsiriX 3.6.1 (OsiriX fondation, Geneva, Switzerland). A first set of points was applied in each DICOM series (CT and MRI) on consistent anatomical landmarks, and registration accuracy was then assessed on a fused series, with MRI data overlaid on CT images, by measuring the distance between the 2 endocardial borders. In case this distance was above 1 mm, additional points were added in the 2 series, and then registration and fusion were applied again until sub-millimetric accuracy was reached. Myocardial and vascular structures were segmented on the MDCT series. Scar and GZ were segmented from the registered MRI series using an adaptative thresholding algorithm developed as an OsiriX plugin. Scar and GZ thresholds were defined at 50 to 100% and 35 to 50% of maximal myocardial signal, respectively (17,18). Segmented images were used to generate 3D surface meshes of the endocardium, epicardium, coronary arteries, CS, scar and GZ, using the software CardioviZ3D (Asclepios Team, INRIA Sophia Antipolis, France). Areas of scar and GZ in contact with endocardial and epicardial surfaces were computed from MRI data. Areas of WT were computed from MDCT data, and displayed on both endocardial and epicardial surfaces. The 5 mm value was used as a cut-off to define wall thinning based on previous reports of LV end-diastolic wall thickness in a healthy population (19). The resulting 3D objects were imported into 3D-mapping systems (EnSite NavX, St Jude Medical,

St. Paul, MN; CARTO 3, Biosense Webster, Diamond Bar, CA). All imaging models were available for real time guidance during the subsequent EP procedures.

Mapping/Ablation

3D-electroanatomical mapping was performed through a combined endocardial (via both trans-septal and retrograde aortic access), and pericardial approach. NavX mapping procedures were acquired using a 20-pole five-spline catheter (PentaRay, Biosense Webster, Diamond Bar, CA). CARTO procedures were acquired using a 3.5mm irrigated-tip catheter (Navistar ThermoCool, Biosense Webster, Diamond Bar, CA). The pericardial geometry with simultaneous acquisition of sinus rhythm activation was first performed, then a complete endocardial mapping geometry was acquired including the CS, left atrium (with its 4 pulmonary veins and left atrial appendage), mitral annulus, left ventricular endocardium and aortic root. Point-based registration with the imaging model was initiated using a first set of coupled points on the above-mentioned landmarks. When using NavX platform, registration was refined during endocardial and epicardial mapping using additional landmarks on LV and RV free walls. When using CARTO platform, registration was refined using automatic surface registration. In addition, a 6F decapolar catheter (Xtreme, Sorin, France) was placed in the CS as distally as possible. This catheter was used as a spatial reference to detect potential shift of the map throughout the procedure (Figure 2). Inducibility of VT was tested using programmed RV stimulation (1-4 extrastimuli). When VT was inducible and hemodynamically tolerated, ablation was performed with the guidance of conventional activation and entrainment mapping. After the restoration of sinus rhythm, LAVA were ablated with the endpoint of elimination. If VT was still inducible using the same stimulation protocol, it was remapped and LAVA were again looked for. The procedural endpoint was complete elimination of LAVA and non-inducibility. In patients with poorly tolerated or non-

inducible VT, LAVA were targeted by ablation with the endpoint of complete elimination and non-inducibility.

Data Analysis

Bipolar electrograms were filtered at 30 to 400 Hz. Post-hoc analysis was performed by one observer (YK) in order to validate each electrogram with respect to contact quality, and to categorize each mapping site as either normal or abnormal. A threshold of 1.5mV was used to define low voltage (6,9). Areas of low voltage were manually traced on the model, and compared to areas of DE and WT. LAVA were defined as 1) sharp high frequency ventricular potentials possibly of low amplitude, 2) distinct from the far field ventricular electrogram, 3) occurring anytime during or after the far field ventricular electrogram in sinus rhythm or before the far field ventricular electrogram during VT, 4) that sometimes displayed fractionation, double or multiple components separated by very low amplitude signals or an isoelectric interval, and 5) were poorly coupled to the rest of the myocardium (8). The number of LAVA, ablation sites, and critical isthmuses sites projecting inside and outside areas of DE and WT was assessed. When outside, the distance to the area border was measured.

Statistical Analysis

Continuous variables are expressed as mean±SD. Categorical variables are expressed as frequency (%), fraction when appropriate. The performance of DEMRI and CT-WT for the detection of low voltage is assessed by measuring the area of overlap. Areas are expressed in cm^2, and normalized to low voltage area.

RESULTS

Patient characteristics are summarized in Table 1.

Feasibility of the registration process

Co-registration between MDCT and MRI was feasible in all patients with sub-millimetric accuracy. Integration of fused MDCT-MRI data in catheter localization platforms was feasible in all patients, enabling real time 3D visualization of endocardium, epicardium, scar core, GZ, WT and coronary vessels during VT mapping/ablation. CS successfully monitored registration accuracy during the procedure in all patients. Coronary arteries were successfully used to guide epicardial RF delivery in all 7 patients in whom it was performed, provided stable registration as demonstrated by the decapolar catheter placed in an adjacent CS branch. No coronary angiography was performed when ablating more than 1 cm away from the closest coronary artery on MDCT. Endocardial mapping was performed in all patients, and epicardial mapping in 6/8 patients. After exclusion of sites with insufficient contact, endocardial and epicardial mapping densities were 391±388 and 1098±734 points/map, respectively. A total number of 11204 high quality electrograms were reviewed for LAVA identification. The average processing time for the preparation of imaging models for the procedures was typically of 1h. The average processing time for the post hoc analysis of structure-function relationships (LAVA identification, area and overlap measurements on the registered EP and imaging datasets) was 24h per patient.

DEMRI vs Voltage

Low voltage was found in all patients. DE was present in 7/9 patients (3 ICM, 1 NICM, 2 myocarditis, 1 idiopathic VT with previous ablation). The distribution of DE areas with respect to low voltage is presented in Table 2. In ICM patients, DE areas matched areas of low voltage, with an overlap of 91±8 and 94±6 % for scar and scar+GZ, respectively (Figure 3). In NICM patients, DE was only found in 1/3 patient, with poor overlap with low voltage (57 and 59 % for scar and scar+GZ areas, respectively). In patients with myocarditis, sub-

epicardial DE matched epicardial low voltage with an overlap of 83±24 and 92±12 % for scar and scar+GZ areas, respectively. In the patient with idiopathic VT and history of previous ablation, DE was found in the sub-endocadium of both ventricles, as well as in the RV sub-epicardium. Low voltage areas were found larger than DE areas (50 vs 26 cm^2, respectively). The overlap between low voltage and DE was found good in the endocardium (78 and 94% for scar and scar+GZ, respectively), but poor in the epicardium (21 and 27%, respectively) because of a wide area of RV epicardial low voltage that did not correspond to DE (>25 cm^2).

CT-WT vs Voltage

WT was present at CT in 6/9 patients (3 ICM, 3 NICM). The distribution of WT areas with respect to low voltage is presented in Table 2. In ICM patients, WT areas matched areas of low voltage, with an overlap of 79±5 %. In NICM patients, WT areas matched areas of low voltage, with an overlap of 63±21 % (Figure 4). In patients with myocarditis, no WT was found at CT, despite the presence of LV epicardial low voltage. In the patient with idiopathic VT, no WT was found at CT, despite the presence of RV endo- and epicardial low voltage.

DEMRI vs CTWT

In ICM patients, WT and DE were found in all patients. DE area was found larger than WT area (81.8±31.2 vs 60.3±31.6 cm^2, respectively). The overlap was 99% of WT area. In NICM patients, WT was found in all patients, and DE in one. In this patient, DE area was found smaller than WT area (107.7 vs 133 cm^2, respectively). The overlap was 88% of DE area. In patients with myocarditis and in the one with idiopathic VT and previous ablation, no WT was found at CT despite the presence of DE at MRI.

Distribution of ablation targets according to substrate

Ablation was performed in all patients (6/9 endocardially, 7/9 epicardially). VT was mappable in only 1 patient with NICM. The ablation site associated to VT termination was located in an area of WT. In other patients, the procedural endpoint was complete elimination of LAVA and non-inducibility. VT was inducible in 4/9 patients, and a total of 266 LAVA sites were found in 7/9 patients (3 ICM, 2 NICM, 2 myocarditis). Complete elimination of LAVA was obtained in 5/7 patients (2 ICM, 1 NICM, 2 myocarditis). All inducible patients were found non-inducible at the end of the procedure. The distribution of LAVA according to substrate is presented in Table 3, and illustrated in Figure 5. In patients exhibiting low voltage (7/7), the number of LAVA sites associated to low voltage was 235/266 (88±10% of sites). In patients exhibiting DE at MRI (6/7), the number of LAVA sites associated to scar or GZ was 212/226 (95±6%). 100% of LAVA sites were located within 14 mm of GZ border (Figure 6). In patients exhibiting WT at CT (5/7), the number of LAVA sites associated to WT was 153/197 (76±9%). 100% of LAVA sites were located within 18 mm of WT areas border. The total number of LAVA sites associated with the presence of any substrate at imaging (DE at MRI or WT at CT) was 237/266 (90±14%).

DISCUSSION

The main findings of this study are (i) integration of fused MDCT and MRI data for the guidance of VT ablation is feasible, (ii) coronary arteries CT angiography can be used to guide epicardial ablation, (iii) CS CT angiography can be used to monitor image registration during the procedure, (iv) MDCT and MRI provide complementary information on VT substrate that spatially correlates to the electrophysiological substrate.

Integration of fused MDCT-MRI data in 3D mapping systems

Previous studies have reported an integration of scar imaging data in clinical mapping systems. The authors used either PET/CT (20,21) or DEMRI (9,11,12,22) to display 3D scar

maps during VT ablation procedures. Because the spatial resolution of both PET and routine breath-hold DEMRI sequences are limited, we chose to use a free-breathing method to assess DE at high spatial resolution (16). This resulted in a better visual analysis of scar contours, intra-myocardial situation and isthmuses during the procedure. In addition, we chose to merge MRI data with contrast-enhanced cardiac-gated MDCT in order to embed the scar information in a high-resolution 3D-reconstructed anatomic model. CT data simplified the registration process by providing multiple anatomical landmarks that could be used to perform initial registration, and to monitor registration accuracy during the procedure, through the visualization of a catheter placed in a distal CS branch. Last, the integration of CT angiographic data allowed for the visualization of coronary arteries to prevent radio-frequency delivery within a centimeter during epicardial ablation. A closer ablation site would have been investigated with direct coronary angiogram but one can understand that this cannot be repeated for every epicardial RF delivery. The advantage of a submillimetric coronary artery reconstruction registered to the navigation system is then obvious. This holds true to prevent RF delivery on the left phrenic nerve as well, this structure being visible on MDCT images.

DEMRI and voltage mapping

Using the usual bipolar threshold of 1.5mV to define low voltage, we found a match between DEMRI and low voltage in 3 patients with ICM, and 2 patients with myocarditis. However, areas of DE were consistently found larger than areas of low voltage. This is consistent with previous studies reporting an underestimation of voltage-defined scar as compared to DEMRI in ischemic patients (12). It is to our knowledge the first report on the spatial correlation between low voltage and DE in post-myocarditis scar. In the patient with idiopathic VT and history of previous ablation, prior knowledge of previous ablation sites helped focusing the mapping on its border areas. However we found poor correlation between DE and low voltage

in this patient, mainly because of a large area of epicardial low voltage on the RV, which did not correspond to DE. This might be explained by the lower specificity of epicardial voltage mapping on the RV using standard voltage thresholds, because of thinner myocardium and thicker epicardial fat (23). This hypothesis is supported by the fact that this patient had a good match between DE and low voltage on the RV endocardium (overlap 94%). Last, correlation between low voltage and DE in NICM patients was poor, DE being found in only 1 patient. This is likely to be due to the limitations of inversion-recovery MR pulse sequences for the depiction of diffuse interstitial remodeling (13).

CT-WT and voltage mapping

Using a 5 mm cut-off to define significant left ventricular WT, we found a substantial match between WT and low voltage in patients with ICM, as well as in patients with NICM. This is consistent with a previous report by Tian et al in ischemic patients (14). The underlying hypothesis is that interstitial remodeling in both ischemic and non-ischemic dilated cardiomyopathies is characterized by cellular loss and collagenase activation that affect myocardial thickness (24). This could be of value to locate the structural substrate of VT in patients with structural heart disease but no DE at MRI, as well as in patients with ICDs in whom MRI cannot be performed.

Distribution of ablation targets according to substrate

In this study, most VTs were not accessible to mapping, and ablation strategy focused on LAVA with the endpoint of complete elimination and non-inducibility. Persistent electrical activity within scar indicates the presence of surviving myocyte bundles within fibrosis (25,26). These sites are characterized by slow conduction, which is the substrate for re-entry (3,27), and are therefore promising targets for the ablation of un-mappable scar-related VT (7,8,28). There is to our knowledge no previous report in the literature on the relationship

between LAVA and structural substrate as assessed with imaging. This study shows that the vast majority of sites exhibiting LAVA are associated to structural abnormalities (90% inside an abnormal area, 100% within 18mm), DE at MRI being the most accurate feature in ischemic patients, and WT at CT in non-ischemic patients.

Complementarities between CT and MRI

The addition of MDCT data on WT might provide information on VT substrate that is complementary to DEMRI. In this study, ICM patients exhibited both DE and CT-WT in sites of prior transmural myocardial infarction. NICM patients exhibited WT at CT but no, or few, DE. The 2 other patients with myocarditis and idiopathic VT exhibited DE but no WT at CT. When present, DE was the most accurate imaging feature for the identification of low voltage (mean overlap 80%) and LAVA sites (95% of LAVA inside DE areas, 100% within 14mm). However, most patients with non-ischemic dilated cardiomyopathy do not show DE at MRI because the method cannot depict diffuse interstitial remodeling (13). This study suggests that in these patients, CT-WT might provide a localization of both low voltage (mean overlap 63%) and LAVA sites (72% of LAVA inside WT areas, 100% within 18mm). This complementarity between DE and WT is supported by our results in the total population, with a number of detected LAVA sites increasing from 80% (212/266) to 90% (237/266) when adding CT-WT to DEMRI data.

Study limitations

The main limitation of this study is its small sample size due to ICD precluding MRI. In addition, our results on structure-function relationships might be limited by the variety of underlying diseases in the studied population. However, the objectives of this study were to demonstrate the feasibility and usefulness of the multimodal approach rather than to validate each imaging parameter for the identification of VT substrate. We chose to study a population

that resembles the general population referred for VT ablation, and our results illustrate how such a multimodal approach can accommodate to different clinical settings. Further studies on larger populations are needed to confirm our results on CT-WT and DEMRI parameters and to define consistent thresholds in both ischemic and non-ischemic patients. Particularly, the performance of WT for the detection of low voltage and LAVA in ischemic patients might have been overestimated in this study because our population mainly showed transmural scar. Indeed, non-transmural infarcts might have less impact on wall thickness. Another limitation is due to the fact that 2 electro-anatomic systems with different catheter localization accuracy and registration methods were used. However, this cross-platform design was chosen to demonstrate the feasibility of the multimodal MDCT-MRI approach on the 2 most widely used clinical systems. Last, another limitation of this study is related to the endpoint of ablation. Even if a detailed definition of LAVA has been reported earlier (8), the intra- and inter-observer reproducibility of LAVA identification, as well as the range of frequency of LAVA signals have not been reported.

CONCLUSION

Multimodal guidance of VT mapping and ablation using fused MDCT and MRI data is feasible and useful. MDCT provides anatomical details facilitating the image integration process. Coronary sinus MDCT angiography enables a real-time monitoring of registration accuracy during the procedure. Coronary arteries MDCT angiography can be used to guide epicardial ablation. DE at MRI and myocardial WT at CT provide complementary information on VT substrate, which spatially correlates to areas of low voltage and local abnormal ventricular activities during sinus rhythm.

ACKNOWLEDGEMENTS

Authors thank Pr N Marrouche, Dr R MacLeod and Dr E Kholmovski for their providing of the MRI pulse sequence for high-resolution scar imaging.

REFERENCES

1. Zipes DP, Wellens HJ. Sudden cardiac death. Circulation. 1998;98:2334-51.
2. Ursell PC, Gardner PI, Albala A, Fenoglio JJ Jr, Wit AL. Structural and electrophysiological changes in the epicardial border zone of canine myocardial infarcts during infarct healing. Circulation Res. 1985;56:436-51.
3. de Bakker JM, van Capelle FJ, Janse MJ et al. Slow conduction in the infarcted human heart: 'zigzag' course of activation. Circulation. 1993;88:915-26.
4. Stevenson WG, Wilber DJ, Natale A et al. Irrigated radiofrequency catheter ablation guided by electroanatomicmapping for recurrent ventricular tachycardia after myocardial infarction: Themulticenter thermocool ventricular tachycardia ablation trial. Circulation 2008;118:2773-82.
5. Soejima K, Suzuki M, Maisel WH et al. Catheter ablation in patients with multiple and unstable ventricular tachycardias after myocardial infarction: short ablation lines guided by reentry circuit isthmuses and sinus rhythm mapping. Circulation 2001;104: 664-69.
6. Marchlinski FE, Callans DJ, Gottlieb CD, Zado E. Linear ablation lesions for control of unmappable ventricular tachycardia in patients with ischemic and non-ischemic cardiomyopathy. Circulation 2000;101:1288-96.
7. Arenal A, Glez-Torrecilla E, Ortiz M et al. Ablation of electrograms with an isolated, delayed component as treatment of unmappable monomorphic ventricular tachycardias in patients with structural heart disease. J Am Coll Cardiol 2003;41:81-92.
8. Jais P, Maury P, Khairy P et al. Elimination of local abnormal ventricular activities: a new end point for substrate modification in patients with scar-related ventricular tachycardia. Circulation 2012;125:2184-96.
9. Reddy VY, Malchano ZJ, Holmvang G et al. Integration of cardiac magnetic resonance imaging with three-dimensional electroanatomic mapping to guide left ventricular catheter manipulation: feasibility in a porcine model of healed myocardial infarction. J Am Coll Cardiol 2004;44:2202-13.

10. Codreanu A, Odille F, Aliot E et al. Electroanatomic characterization of post-infarct scars comparison with 3-dimensional myocardial scar reconstruction based on magnetic resonance imaging. J Am Coll Cardiol 2008;52:839-42.
11. Desjardins B, Crawford T, Good E et al. Infarct architecture and characteristics on delayed enhanced magnetic resonance imaging and electroanatomic mapping in patients with postinfarction ventricular arrhythmia. Heart Rhythm 2009;6:644-51
12. Wijnmaalen AP, van der Geest RJ, van Huls van Taxis CF et al. Head-to-head comparison of contrast-enhanced magnetic resonance imaging and electroanatomical voltage mapping to assess post-infarct scar characteristics in patients with ventricular tachycardias: real-time image integration and reversed registration. Eur Heart J 2011;32:104-14
13. McCrohon JA, Moon JC, Prasad SK et al. Differentiation of heart failure related to dilated cardiomyopathy and coronary artery disease using gadolinium-enhanced cardiovascular magnetic resonance. Circulation 2003;108:54-59.
14. Tian J, Jeudy J, Smith MF et al. Three-dimensional contrast-enhanced multidetector CT for anatomic, dynamic, and perfusion characterization of abnormal myocardium to guide ventricular tachycardia ablations. Circ Arrhythm Electrophysiol. 2010;3:496-504
15. Zeppenfeld K, Tops LF, Bax JJ, Schalij MJ. Images in cardiovascular medicine. Epicardial radiofrequency catheter ablation of ventricular tachycardia in the vicinity of coronary arteries is facilitated by fusion of 3-dimensional electroanatomical mapping with multislice computed tomography. Circulation 2006;114:e51-e52.
16. McGann CJ, Kholmovski EG, Oakes RS et al. New magnetic resonance imaging-based method for defining the extent of left atrial wall injury after the ablation of atrial fibrillation. J Am Coll Cardiol 2008;52:1263-71.
17. Amado LC, Gerber BL, Gupta SN et al. Accurate and objective infarct sizing by contrast-enhanced magnetic resonance imaging in a canine myocardial infarction model. J Am Coll Cardiol 2004;44:2383-89.
18. Roes SD, Borleffs CJ, van der Geest RJ et al. Infarct tissue heterogeneity assessed with contrast-enhanced MRI predicts spontaneous ventricular arrhythmia in patients with ischemic

cardiomyopathy and implantable cardioverter-defibrillator. Circ Cardiovasc Imaging 2009;2:183-90.

19. Stolzmann P, Scheffel H, Leschka S et al. Reference values for quantitative left ventricular and left atrial measurements in cardiac computed tomography. Eur Radiol 2008;18:1625-34
20. Dickfeld T, Lei P, Dilsizian V, Jeudy J et al. Integration of three-dimensional scar maps for ventricular tachycardia ablation with positron emission tomography-computed tomography. JACC Cardiovasc Imaging 2008;1:73-82.
21. Fahmy TS, Wazni OM, Jaber WA et al. Integration of PET/CT with Electroanatomical mapping: A novel approach for ablation of scar-related VT. Heart Rhythm 2008;5:1538-45.
22. Dickfeld T, Tian J, Ahmad G et al. MRI-Guided ventricular tachycardia ablation: integration of late gadolinium-enhanced 3D scar in patients with implantable cardioverter-defibrillators. Circ Arrhythm Electrophysiol 2011;4:172-84
23. Desjardins B, Morady F, Bogun F. Effect of epicardial fat on electroanatomical mapping and epicardial catheter ablation. J Am Coll Cardiol 2010;56:1320-7
24. Gaasch WH, Zile MR. Left ventricular structural remodeling in health and disease : with special emphasis on volume, mass, and geometry. J Am Coll Cardiol 2011;58:1733-40
25. Harada T, Stevenson WG, Kocovic DZ, Friedman PL. Catheter ablation of ventricular tachycardia after myocardial infarction: relation of endocardial sinus rhythm late potentials to the reentry circuit. J Am Coll Cardiol 1997;30:1015-23.
26. de Bakker JM, Coronel R, Tasseron S et al. Ventricular tachycardia in the infarcted, Langendorff-perfused human heart: role of the arrangement of surviving cardiac fibers. J Am Coll Cardiol 1990;15:1594-607.
27. de Bakker JM, van Capelle FJ, Janse MJ et al. Reentry as a cause of ventricular tachycardia in patients with chronic ischemic heart disease: electrophysiologic and anatomic correlation. Circulation 1988;77:589-606.
28. Bogun F, Good E, Reich S et al. Isolated potentials during sinus rhythm and pace-mapping within scars as guides for ablation of post-infarction ventricular tachycardia. J Am Coll Cardiol 2006;47:2013-9.

TABLES

Table 1. Patient characteristics											
Patient	Age	sex	LVEF	Aetiology	Mapping					Substrate at imaging	
					System	Number of points on endocardium	Number of points on epicardium	Low voltage (endo/epi)	LAVA (endo/epi)	DE at MRI (endo/epi)	WT at CT
1	64	F	37	ICM	NavX	1342	1785	+ / +	+ / +	+ / +	+
2	62	M	20	ICM	Carto	151	-	+ / NA	+ / NA	+ / +	+
3	31	M	38	ICM	Carto	175	-	+ / NA	+ / NA	+ / +	+
4	45	M	20	NICM	NavX	470	960	+ / +	- / +	- / -	+
5	54	M	30	NICM	NavX	270	935	+ / +	+ / +	- / +	+
6	57	M	25	NICM	NavX	141	198	+ / +	- / -	- / -	+
7	31	M	50	Myocarditis	NavX	317	1385	- / +	- / +	- / +	-
8	32	M	62	Myocarditis	Carto	102	262	- / +	- / +	- / +	-
9	36	F	60	Idiopathic VT	NavX	551	2160	+ / +	- / -	+ / +	-

ICM: ischaemic cardiomyopathy; NICM: non ischaemic cardiomyopathy; LVEF: left ventricular ejection fraction; VT: ventricular tachycardia; LAVA: local abnormal ventricular activities; DE: delayed-enhancement; WT: wall thinning.

Table 2. Distribution of substrate at imaging with respect to low voltage									
Patient: Aetiology	**MR scar area**	**MR scar+GZ area**	**CT wall thinning area**	**Any substrate area**	**Low voltage area**	**Overlap with MR scar**	**Overlap with MR scar+GZ**	**Overlap with wall thinning**	**Overlap with any substrate**
1:ICM	100.9	116.9	96.2	120.2	110.4	93.0 **(84%)**	97.7 **(88%)**	84.0 **(76%)**	101 **(91%)**
2:ICM	50.4	57.3	47.8	57.3	53.6	47.9 **(89%)**	50.0 **(93%)**	45.7 **(85%)**	50.0 **(93%)**
3:ICM	54.9	71.3	36.9	71.3	40.3	40.3 **(100%)**	40.3 **(100%)**	31.0 **(77%)**	40.3 **(100%)**
4:NICM	-	-	80.8	80.8	82	-	-	60.4 **(74%)**	60.4 **(74%)**
5:NICM	88.5	107.7	133	146.1	136.2	77.5 **(57%)**	81.1 **(59%)**	104.5 **(77%)**	117.6 **(86%)**
6:NICM	-	-	14	14	21.8	-	-	8.6 **(39%)**	8.6 **(39%)**
7:Myocarditis	38.3	73.7	-	73.7	49.9	32.8 **(66%)**	41.2 **(83%)**	-	41.2 **(83%)**
8:Myocarditis	29.2	35.9	-	35.9	5.5	5.5 **(100%)**	5.5 **(100%)**	-	5.5 **(100%)**
9:Idiopathic VT	21.5	26.2	-	26.2	50	16.1 **(32%)**	20 **(40%)**	-	20 **(40%)**
					MEAN	**75 ± 25 %**	**80 ± 23 %**	**71 ± 16 %**	**78 ± 24 %**

Areas are expressed in cm^2 (% of low voltage area). Low voltage: bipolar voltage <1.5mV; Wall thinning: wall thickness <5mm; MR scar: DEMRI signal >50% maximum intensity; MR scar+GZ: DEMRI signal >35% maximum intensity; GZ: grey zone.

Table 3. Distribution of LAVA according to substrate at imaging						
Patient	**Aetiology**	**No. of LAVA sites**	**Low voltage**	**MR scar+GZ**	**CT thinning**	**Any substrate at imaging**
1	ICM	86	80 (93%)	81 (94%)	72 (84%)	81 (94%)
2	ICM	24	24 (100%)	24 (100%)	19 (79%)	24 (100%)
3	ICM	16	14 (87%)	16 (100%)	11 (69%)	16 (100%)
4	NICM	40	36 (90%)	-	25 (63%)	25 (63%)
5	NICM	31	29 (93%)	26 (84%)	26 (84%)	26 (84%)
6	NICM	0	-	-	-	-
7	Myocarditis	34	28 (82%)	33 (97%)	-	33 (97%)
8	Myocarditis	35	24 (68%)	32 (92%)	-	32 (92%)
9	Idiopathic VT	0	-	-	-	-
Total		**266**	**235 / 266 (88±10%)**	**212 / 226 (95±6%)**	**153 / 197 (76±9%)**	**237 / 266 (90±13%)**

Data is expressed as actual number of sites (% of total sites). LAVA: local abnormal ventricular activities.

FIGURE LEGENDS

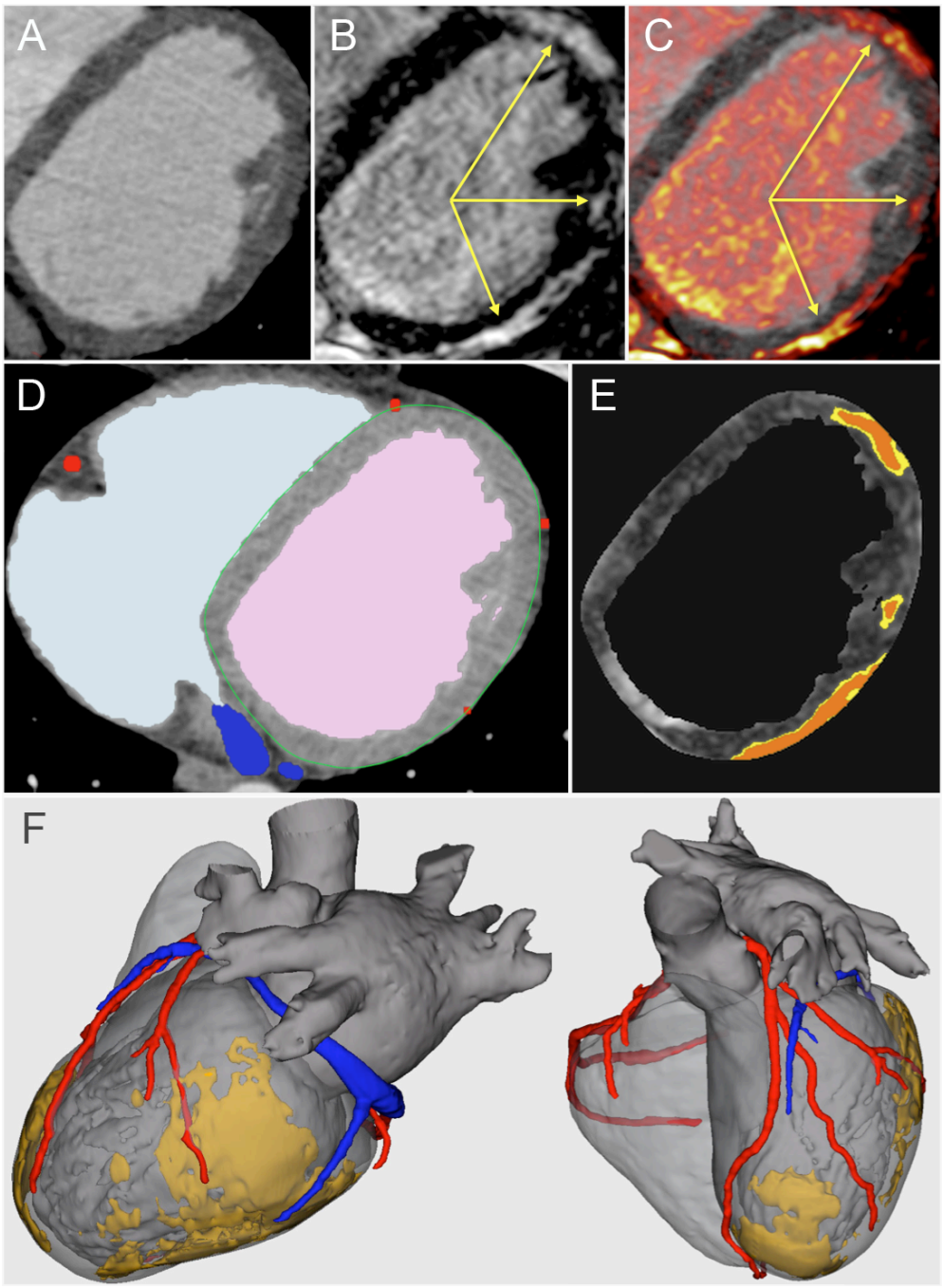

Figure 1: Image post processing. Registration between (a) MDCT and (b) DEMRI images is controlled on (c) a fused series. (d) Cardiac chambers and epicardial vessels are segmented from MDCT data. (e) Myocardial scar and GZ are segmented from MRI data. (f) Segmented images are used to compute patient-specific 3D objects compatible with 3D-mapping systems.

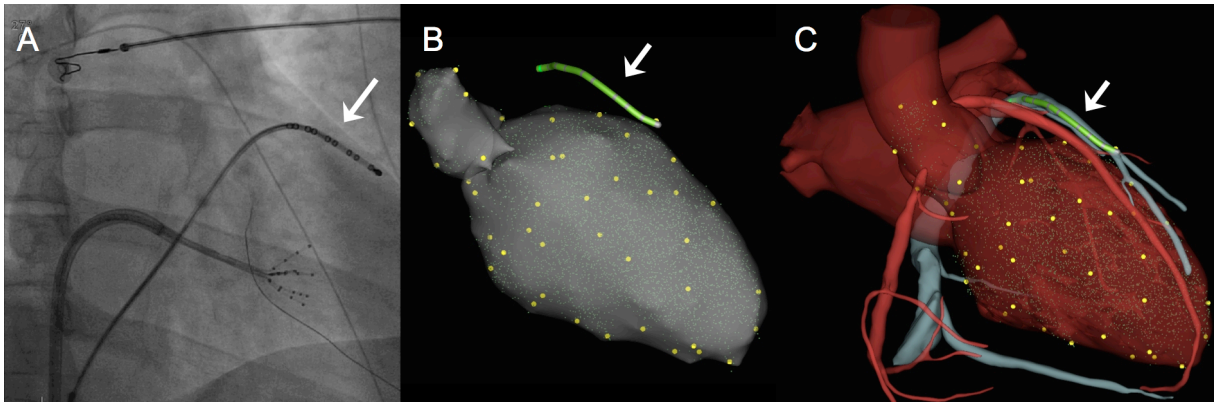

Figure 2: Monitoring the image registration with a CS catheter. A 6F decapolar catheter (Xtreme, Sorin, France) is placed in a distal CS branch (a). This catheter is used as a spatial reference to detect potential shift between the mapping geometry (b) and the imaging model (c) throughout the procedure.

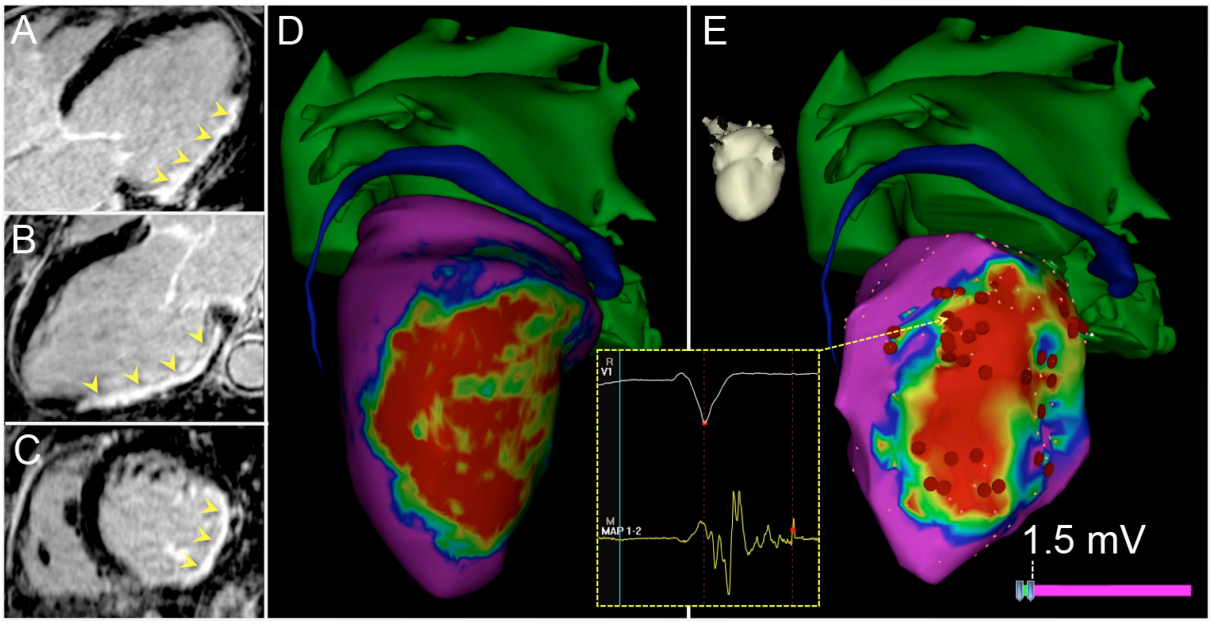

Figure 3: Correlation between voltage and DEMRI in a patient with ischemic cardiomyopathy. DE is seen in the lateral and posterior sub-endocardium on (a) 4-chambers, (b) 3-chambers and (c) short axis reconstructions of the DEMRI 3D volume. (d) The area of scar and GZ in contact with the endocardium is displayed on a detailed MDCT anatomic model integrated in the CARTO system. (e) The endocardial voltage map is registered to the imaging model, demonstrating a match between DE and low voltage. Red dots indicate sites of LAVA targeted by ablation. A complex fractionated signal (yellow frame) made of far field ventricular electrogram and delayed high frequency component is recorded. The high frequency component (red dot) indicates the presence of surviving myocytes surrounded by scar tissue in the vicinity of the catheter tip.

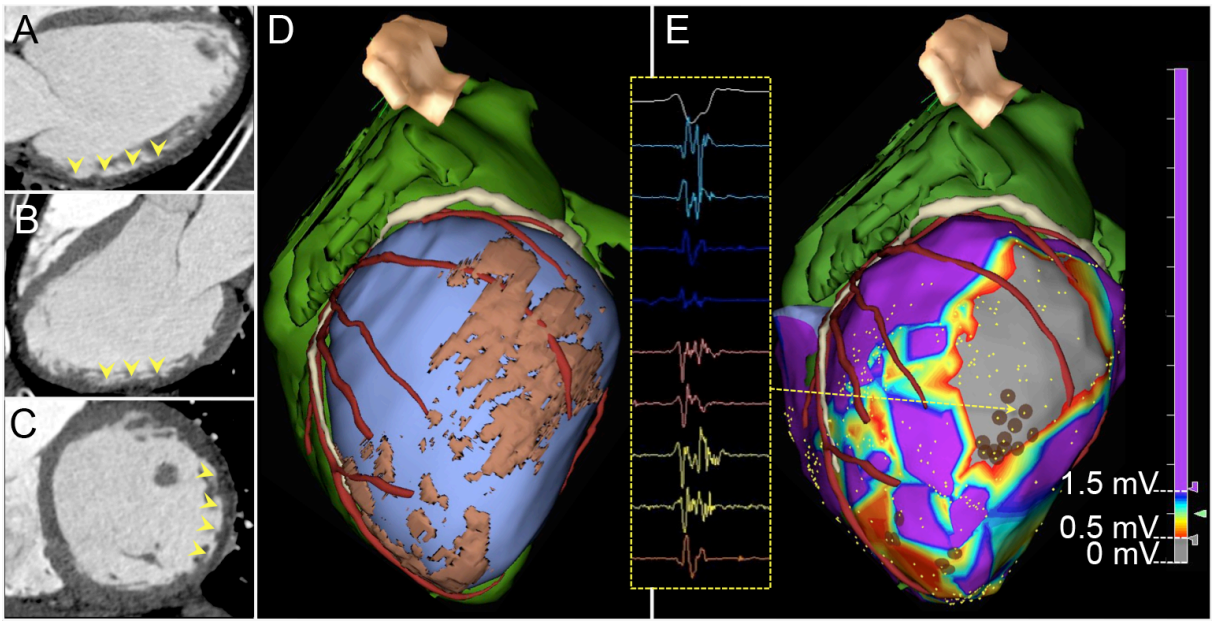

Figure 4: Correlation between voltage and wall thinning at MDCT in a patient with non-ischemic dilated cardiomyopathy. Myocardial wall thinning is seen in the lateral wall of the left ventricle on (a) 4-chambers, (b) 3-chambers, and (c) short axis reconstructions of the contrast-enhanced MDCT volume. No DE was seen at MRI. (d) Areas of wall thickness <5mm are mapped on the epicardial surface and integrated in the NavX system. (e) The epicardial voltage map is registered to the imaging model, demonstrating a match between wall thinning and low voltage. Brown dots indicate sites of LAVA targeted by ablation. A high-frequency fragmented signal occurring during the far field ventricular electrogram is seen (yellow frame), indicating the presence of persisting local electrical activity within scar. Please note that these high frequency signals are fractionated but not late as they are recorded within the QRS.

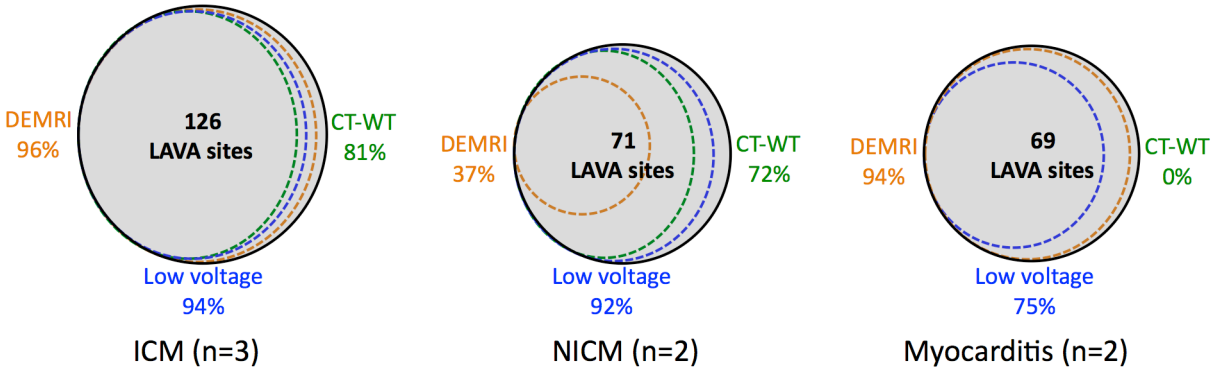

Figure 5: Distribution of LAVA sites according to substrate. The percentages of local abnormal ventricular activity (LAVA) sites projecting inside an area of low voltage at contact mapping, wall thinning (WT) at MDCT, and delayed-enhancement (DE) at MRI are presented according to the underlying disease. ICM: Ischemic cardiomyopathy; NICM: Non ischemic cardiomyopathy.

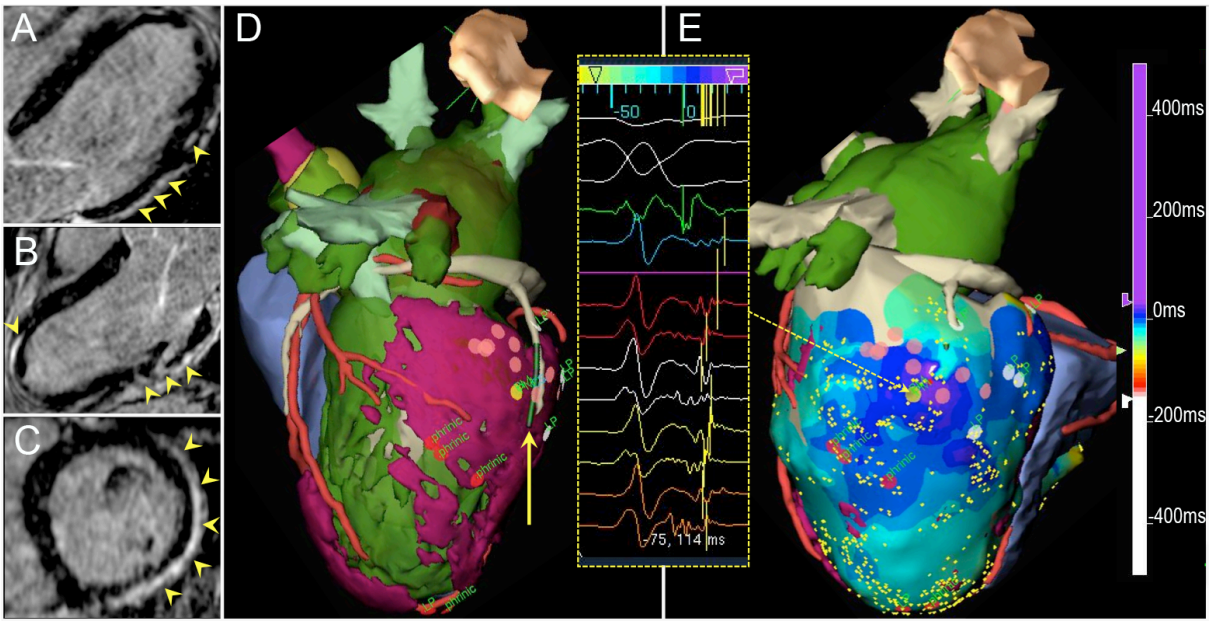

Figure 6: Correlation between epicardial activation and DEMRI in a patient with myocarditis. DE is seen in the lateral, inferior and anterior sub-epicardium of the left ventricle wall on (a) 4-chambers, (b) 3-chambers, and (c) short axis reconstructions of the DEMRI volume. No wall thinning was seen at MDCT. (d) The area of scar and GZ in contact with the epicardium is displayed in the NavX system. (e) The epicardial isochronal map acquired during sinus rhythm is registered to the imaging model, demonstrating a clear match between areas of DE and latest ventricular activity. Pink dots indicate sites of LAVA targeted by ablation. High frequency signals are recorded (yellow frame), occurring late after the far field ventricular electrogram. In this patient, epicardial ablation was performed in the vicinity of several coronary arteries (circumflex, diagonal branch). A catheter was positioned in a posterior-lateral branch of the CS (arrow in image d) to ensure registration stability during RF delivery.